Energy Alignment, Molecular Packing, and Electronic Pathways: Zinc(II) Tetraphenylporphyrin Derivatives Adsorbed on TiO2(110) and ZnO(11−20) Surfaces

ARTICLE *in* THE JOURNAL OF PHYSICAL CHEMISTRY C · NOVEMBER 2012

Impact Factor: 4.77 · DOI: 10.1021/jp307454y

THE JOURNAL OF PHYSICAL CHEMISTRY C

Article

pubs.acs.org/JPCC

Energy Alignment, Molecular Packing, and Electronic Pathways: Zinc(II) Tetraphenylporphyrin Derivatives Adsorbed on TiO_2(110) and ZnO(11−20) Surfaces

Sylvie Rangan,*[,†] Senia Coh,[†] Robert Allen Bartynski,[†] Keyur P. Chitre,[‡] Elena Galoppini,[‡] Cherno Jaye,[§] and Daniel Fischer[§]

[†]Department of Physics and Astronomy and Laboratory for Surface Modification, Rutgers University, 136 Frelinghuysen Road, Piscataway, New Jersey 08854, United States

[‡]Chemistry Department, Rutgers University, 73 Warren Street, Newark, New Jersey 07102, United States

[§]National Institute of Standards and Technology, Material Measurement Laboratory, Gaithersburg, Maryland 20899, United States

ABSTRACT: The relation between energy alignment, adsorption geometry, and electron transfer between a chromophore and an oxide surface has been explored for a series of Zn(II) tetraphenylporphyrin derivatives adsorbed on TiO_2(110) and ZnO(11$\bar{2}$0) surfaces. The electronic occupied and unoccupied structure has been obtained using UV-photoemission and inverse photoemission spectroscopies. From these results, a full picture of the energetics at the chromophore−oxide interface was established. The alignment of the molecular levels relevant for optical transition was found independent of the functionalization of the meso-phenyl groups. However, to explain the observation of different optical properties and electron transfer efficiencies of these different dyes, the adsorption geometry of two of these dyes was determined using scanning tunnel microscopy and near edge absorption fine structure spectroscopy. Functionalization of the meso-phenyls with COOH groups in the meta-position results in the ZnP macrocycle adsorbed parallel to the surface. Functionalization of the meso-phenyl groups with COOH groups in the para position results in a bounding geometry where the ZnP macrocycle makes an angle of ∼50° from the surface normal. This geometry, which allows face-to-face stacking of the porphyrin rings, opens a new electronic channel for exciton delocalization that competes with direct electron injection into the substrate conduction band.

INTRODUCTION

Due to their superior light absorption properties, large molar absorption coefficients, and highly tunable photophysical properties,[1] porphyrins interfaced with wide band gap semiconductors have received considerable attention as promising chromophores for solar-energy applications.[2−33] This interest is motivated by the variety of synthetic modifications to which porphyrin are amenable: functionalization of the macrocycle,[1,8−11,14−16,32] introduction of linker units for the attachment on surfaces,[8−12,14−16,24,26,32] or variation of the metal center.[1,8,9] Active efforts in porphyrin modifications have recently led to an unprecedented power conversion efficiency exceeding 12% in an optimized dye sensitized solar cell (DSSC).[32] Other approaches such as covalent or self-assembly strategies have also been used to form multiporphyrinic arrays[21,23,28] or arrays with complementary chromophores, such as perylene-imides[7,30] or Ru complexes[17,20] (which increase light harvesting in the blue-green region where porphyrins are weak absorbers). Furthermore, multiporphyrinic arrays have been proposed for the design of new "thin" solar cell configurations,[13] that involve planar semiconductor surfaces. Porphyrin-based molecules have also been used to fabricate nanoscale devices using "bottom-up" strategies, for the self-assembly or synthesis of antennas in artificial photosynthetic systems,[2−4] and as key components of new types of photocatalysts.[34]

A critical consideration in all these applications is the nature of the interface between the first molecular layer and the substrate surface. The adsorption geometry at the surface, the molecule−molecule interactions, the resulting electronic structure, and the energy alignment of the molecular levels with respect to the substrate band structure are of primary importance, as they shape the electronic pathways between the molecular adsorbate and the substrate.

In the particular case of the porphyrins, light absorption can be thought of, in the simplest approximation, as the transition of an electron from the HOMOs to the LUMOs of the molecule. For efficient charge separation, the energy of the LUMOs should be above the conduction band minimum of the semiconductor substrate and the HOMOs should be in the substrate band gap, at an energy below the redox potential of the electrolyte. Over the years, major channels that compete with electron transfer in DSSCs have been characterized, such as chromophore deexcitation, conduction band electron capture by the redox-mediator, or back electron transfer on the chromophore cation.[32,35] In the case of porphyrin derivatives, chromophore aggregation at the surface is also believed to create new electronic deexcitation pathways,

Received: July 27, 2012
Revised: October 18, 2012
Published: October 23, 2012

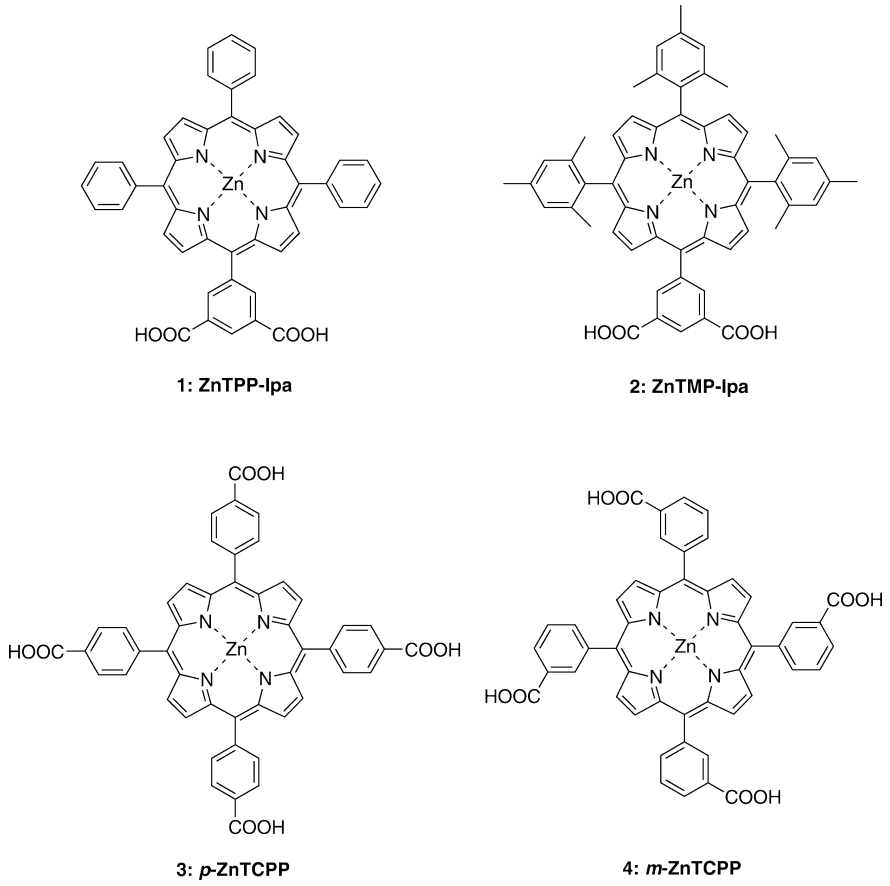

Figure 1. The four ZnTPP derivatives considered in this study.

through dipole/dipole interaction,[36] that compete with direct charge transfer to the substrate conduction band.[18,37,38]

A major obstacle impeding understanding of local electronic phenomena at the chromophore−surface interface is the absence of direct measurements of the chromophore adsorption geometry and the associated implications on the optical absorption properties of the system. Most attempts at directly characterizing these properties have been aimed at small molecules meant to represent portions of a larger chormophore. Near edge X-ray absorption fine structure spectroscopy has been applied to adsorbed small linker groups, and the results were then extrapolated to deduce the possible molecular orientation of larger adsorbates.[39,40] Experimental determination of the vibrational properties of anchoring groups has provided indirect evidence of possible bonding modes.[41−43] The geometry of larger chromophores at surfaces have been indirectly inferred from UV−visible absorption spectroscopy[18,37,38] and from a measure of the dye monolayer thickness,[44,45] although chromophore orientation has been extracted from vibrational spectroscopy in mixed overlayers on gold.[46] Theoretically, calculations addressing large adsorbates and molecule−molecule interactions remain computational challenges. Ab initio approaches have focused on small molecules, determining preferential anchoring groups and local orientation and predicting the extent of molecular hybridization to the oxide surface.[42,47−51]

In this work, the adsorption geometry and the electronic structure of the chromophore−substrate interface are directly probed and compared to UV−visible absorption properties and resulting electron transfer efficiency. The occupied and unoccupied electronic structure (particularly the HOMO and LUMO energy alignment with respect to the substrate band edges) of four ZnTPP derivatives on the single crystal $TiO_2(110)$ and $ZnO(11\bar{2}0)$ surfaces has been studied using a combination of X-ray and UV photoemission spectroscopies (XPS and UPS) and inverse photoemission spectroscopy (IPS) in a single ultrahigh vacuum (UHV) chamber. The full energy diagram of the chromophore−surface interface has been extracted from the experimental electronic structure with the aid of density functional theory (DFT) calculations. In addition, the adsorption geometries of two representative chromophores (*p*- and *m*-ZnTCPP) have been explored using near edge X-ray absorption spectroscopy (NEXAFS), and supplemented with scanning tunneling microscopy (STM) as a local probe on the $TiO_2(110)$ surface. Our results illustrate the need for a comprehensive approach toward the characterization of these complicated chormophore/semiconductor interfaces, and show that the presence of optical absorption features associated with H-aggregates on the surface are directly correlated with molecules binding in an upright geometry, enabling molecule−molecule dipolar interaction.

EXPERIMENTAL SECTION

Molecules. The four Zn tetraphenylporphyrin derivatives (ZnTPP-Ipa, ZnTMP-Ipa, *p*-ZnTCPP, and *m*-ZnTCPP)[52] used in this study are shown in Figure 1. The synthesis details of the ZnTPP derivatives is described elsewhere.[18,19,22] For characterization using surface science techniques, these molecules were chemisorbed onto single crystal surfaces ($ZnO(11\bar{2}0)$ and $TiO_2(110)$) using solution sensitization. *p*- and *m*-ZnTCPP

dx.doi.org/10.1021/jp307454y | J. Phys. Chem. C 2012, 116, 23921−23930

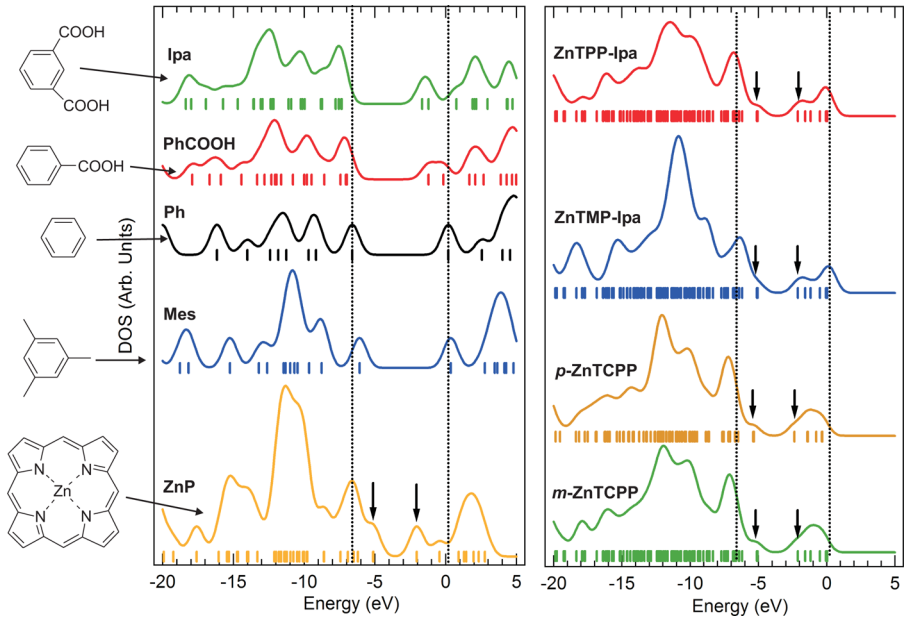

Figure 2. Calculated DOS for the Ipa, PhCOOH, Ph, Mes, and ZnP moieties compared to the calculated DOS of the ZnTPP derivatives considered here. In both graphs, the pairs of arrows indicate the nearly degenerate HOMO-1/HOMO and LUMO centroid positions of a ZnP molecule. The dashed lines are aligned with the degenerate HOMOs and LUMOs of a benzene molecule.

were chosen for NEXAFS, as they have very similar electronic structures but are expected to display drastically different adsorption geometries owing to the para- or meta-positions of the carboxylic acid anchor groups.[18,19,22] UV−vis and IPCE studies were performed on sensitized oxide nanoparticle films.

Sample Preparation. The rutile TiO_2 sample was a commercially produced single-crystal from MTI corporation, cut to within 0.5° of the (110) plane. The ZnO samples were either an epitaxial chemical vapor deposition (CVD) grown film on an Al_2O_3 substrate with the *c*-axis of the film lying in the plane and the $(11\bar{2}0)$ surface exposed or a commercially produced single-crystal from MTI corporation, cut to within 0.5° of the $(11\bar{2}0)$ plane. All samples were degassed and prepared in an ultrahigh vacuum using several cycles of 1 keV Ar^+ ion sputtering (while maintaining a maximum sample current of 2 μA) and annealing in UHV at 900 K for TiO_2 and 800 K for ZnO. The cleanliness of the surfaces was checked using XPS, and the surface termination was assessed by low energy electron diffraction. Following an ex situ 20 min sensitization in a solution of dye in anhydrous ethanol and rinsing with anhydrous ethanol to prevent dye accumulation, the sample was reintroduced into the UHV analysis chamber.

Spectroscopic Methods. Ultraviolet photoemission spectroscopy and inverse photoemission spectroscopy measurements were performed in a single UHV experimental system described elsewhere.[53] In UPS and XPS, the kinetic energy distribution of electrons ejected by excitation from monoenergetic photons reflects the density of occupied states in the system. In IPS, a monoenergetic beam of electrons is directed to the sample and a small fraction undergoes optical decay emitting photons. The resulting photon energy distribution reflects the density of unoccupied states in a manner that is highly complementary to UPS. Core levels were probed using X-ray photoemission spectroscopy excited by non-monochromatized Al Kα radiation, and the valence band electronic states were examined using He II (40.8 eV) excited ultraviolet photoemission spectroscopy. In both cases, electron energy distributions were measured using a cylindrical mirror analyzer. The conduction band spectra were obtained from inverse photoemission spectroscopy, performed using a grating spectrometer with a primary electron energy of 20.3 eV. The overall energy resolution for the UPS and IPS spectra is estimated to be better than 0.3 and 0.6 eV, respectively. The energy scales of the UPS and IPS spectra were calibrated using the measured position of the Fermi level of a gold sample in contact with the oxide sample. NEXAFS spectra were calibrated using a graphite sample.

For both the clean and sensitized surfaces, the secondary electron cutoff has been measured on biased samples using He I (21.1 eV) to determine the electron affinity, given by EA = $h\nu - W - E_{gap}$, where $h\nu$ is the photon source energy, W the total width of the spectra, and E_{gap} is the experimentally measured gap of the oxide surfaces or the molecular gap.

The angle-dependent NEXAFS experiments were performed at the U7A beamline of the National Synchrotron Light Source. NEXAFS is an area-averaging probe well-suited to probing the organization of chemisorbed adsorbates on ordered surfaces.[54] It involves photoexcitation of a core photoelectron to the lowest-lying unoccupied states of the molecule. For the molecules probed here, the former may be the C 1s or N 1s levels, and the latter are the LUMOs on the porphyrin macrocycle or, at slightly higher energy, the π^* system of the phenyls. As a core electron is involved, the spectrum contains information local to the excited atom within the molecule. The ZnTPP derivatives possess four equivalent N sites, all on the porphyrin macrocycle. In principle, there are five inequivalent C sites,[55,56] but the energy splitting among them is small enough to be neglected here. Thus, the N 1s edge spectra will characterize the central porphyrin ring and the C 1s spectra will probe both the porphyrin ring and the meso-phenyls.[55,56] Moreover, when the exciting radiation is linearly polarized, the intensity of an absorption peak depends upon the angle between the photon polarization direction and the orientation of the unoccupied orbitals into which the transition is made.

dx.doi.org/10.1021/jp307454y | J. Phys. Chem. C 2012, 116, 23921−23930

Thus, by monitoring the intensity changes of a spectral feature as a function of polarization orientation (the so-called dichroism), the orientation of the molecule with respect to the plane of the surface can be determined.[57] In order to study the adsorption geometry effects without the complication of differing electronic structures, we have restricted our NEXAFS study to *p*-ZnTCPP and *m*-ZnTCPP: two ZnTPP derivatives that possess essentially the same DOS but for which the position of the COOH groups is expected to lead to different adsorption modes.

Scanning Probe Microscopy. The STM measurements were performed on an Omicron VT-STM and an Omicron LT-STM at either 300 or 90 K. Due to the solution-sensitization approach used in this study, the pristine oxide surfaces have to be removed from the UHV chamber. This step complicates STM measurements, as unwanted adsorbates can profoundly alter imaging. To address this issue, we have dosed the $TiO_2(110)$ surface with pivalic acid vapors in the UHV chamber after preparing an atomically flat and well-ordered surface. This step forms a well-ordered pivalate layer (as verified by STM images, see below) that acts as a robust passivation layer, protecting the surface from atmospheric contaminations while allowing COOH functionalized dyes to replace the pivalate layer in a solution of dye.[58,59] We have adopted this approach with both the *m*-ZnTCPP and *p*-ZnTCPP dyes in order to study the adsorbate geometry at low molecular coverage and thus identify individual adsorbed species.

Computational Methods. Electronic structure calculations of the gas phase molecules were performed with the GAMESS(US) software package[60] using the Becke3–Lee–Yang–Parr (B3LYP) three parameter DFT theory.[61−63] Geometries of local minima on the potential energy surface were calculated with a 6-31G* basis set for nitrogen, carbon, and zinc.[64] The H ligands were described by a 6-31G basis.[64] The density of states (DOS) was produced by performing a sum of the individual electronic states convoluted with a 1 eV full width at half-maximum Gaussian function.

RESULTS AND DISCUSSION

Energy Level Alignment. *Ab Initio Electronic Structure.* Calculations of the molecular geometry for the four dyes were carried out in a fixed symmetry (C_{2v} for ZnTPP-Ipa, C_s for ZnTMP-Ipa, C_{4v} for *p*-ZnTCPP, and *m*-ZnTCPP) within the basis set and functional employed here and give results in good agreement with previous work on similar molecules.[65−67] In all cases, the phenyl groups are found perpendicular to the main ZnP ring, consistent with a weak electronic coupling between the ZnP macrocycle and the outer phenyls. Owing to this weak coupling, we also compared the DOSs corresponding to the different moieties that constitute these ZnTPP derivatives to the DOS obtained for the ZnTPP derivatives, as shown in Figure 2. The positions of the individual energy levels are indicated by markers below each DOS curve. In both graphs, the vertical dotted lines are aligned with the center position of the first occupied and first unoccupied degenerate states (at −6.60 and +0.19 eV, respectively) of a benzene ring (Ph). Similarly, the two arrows indicate the position of the nearly degenerate HOMO-1/HOMO and degenerate LUMOs calculated for the ZnP molecule. The calculated positions of the ZnP and ZnPP derivative frontier orbitals are reported in Table 1.

It is clear that the frontier orbitals of the ZnTPP derivatives can be attributed to the corresponding frontier orbitals of ZnP. The set of states just lower in energy than the HOMOs and just higher in energy than the LUMOs are primarily phenyl-derived. Moreover, the relative energy of the phenyl levels is sensitive to the electron donating (CH_3) or withdrawing (COOH) character of the substituents: the frontier orbitals of $Ph(CH_3)_3$ are shifted toward higher energy, and those of Ph(COOH) and $Ph(COOH)_2$ are shifted toward lower energy, compared to the corresponding states of Ph. These shifts are precisely what is expected from simple electrostatic considerations.

Table 1. Calculated Frontier Orbital Energies in eV and Their Respective Symmetry

molecule	*E*(HOMO-1)	*E*(HOMO)	*E*(LUMO)	*E*(LUMO+1)
ZnP (D_{4h})	−5.12 (a_{2u})	−5.11 (a_{1u})	−2.04 (e_g)	−2.04 (e_g)
ZnTPP-Ipa (C_{2v})	−5.11 (a_2)	−5.06 (b_2)	−2.12 (a_2)	−2.11 (b_2)
ZnTMP-Ipa (C_s)	−5.11 (a″)	−5.01 (a′)	−2.11 (a″)	−2.09 (a′)
p-ZnTCPP (C_{4v})	−5.38 (a_2)	−5.33 (a_1)	−2.37 (e)	−2.37 (e)
m-ZnTCPP (C_{4v})	−5.23 (a_2)	−5.18 (a_1)	−2.23 (e)	−2.23 (e)

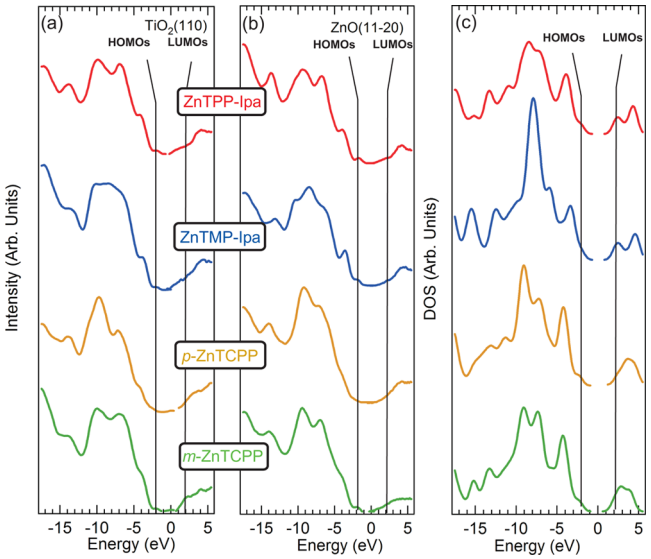

Figure 3. Molecular contribution to the valence band spectra measured in UPS (energy < 0) and conduction band spectra measured in IPS (energy > 0), extracted from sensitized (a) $TiO_2(110)$ and (b) $ZnO(11\bar{2}0)$ surfaces. The energy scale is referenced to the Fermi level of the system. (c) Rescaled calculated DOS for each ZnTPP derivative.

Table 2. HOMO-1/HOMO and LUMO Centroids Extracted from the Experimental Spectra Measured on Sensitized $TiO_2(110)$ and Resulting Energy Gap[a]

molecule	*E*(HOMOs)	*E*(LUMOs)	E_g
ZnTPP-Ipa	−1.8 ± 0.1	2.3 ± 0.1	4.1 ± 0.2
ZnTMP-Ipa	−1.9 ± 0.1	2.3 ± 0.1	4.2 ± 0.2
p-ZnTCPP	−1.9 ± 0.1	2.3 ± 0.1[69]	4.2 ± 0.2[69]
m-ZnTCPP	−1.9 ± 0.1	2.3 ± 0.1[69]	4.2 ± 0.2[69]

[a]All energies are given in eV and referenced with respect to the Fermi level of the system.

dx.doi.org/10.1021/jp307454y | J. Phys. Chem. C 2012, 116, 23921−23930

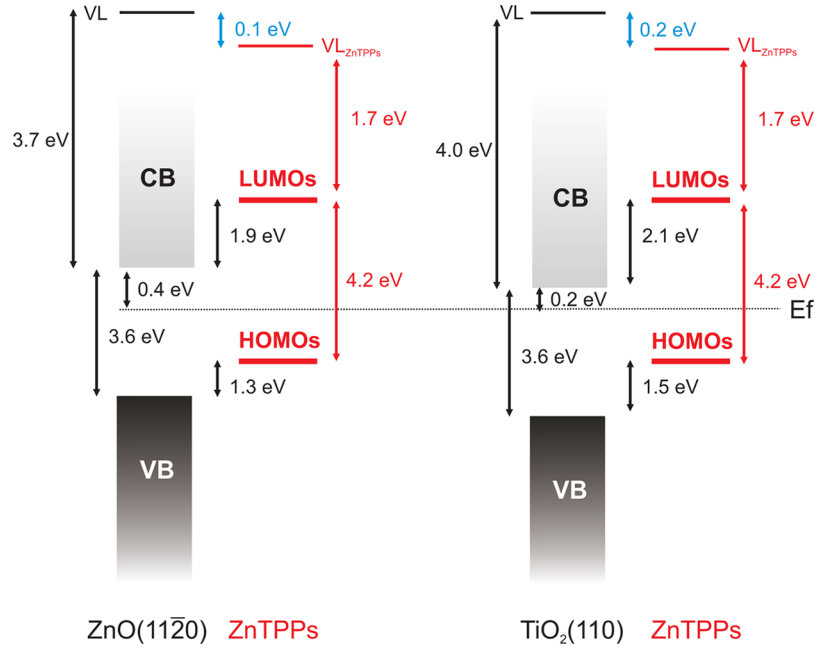

Figure 4. Energy diagram at the ZnTPP/oxide interface for $TiO_2(110)$ and $ZnO(11\bar{2}0)$.

The apparent decoupling of the porphyrin- and phenyl-derived states raises the question as to whether functionalization impacts the light absorption properties of these ZnTPP derivatives, which are closely related to those of ZnP. These systems are generally understood in terms of the Gouterman four-orbital model where states on the porphyrin macrocycle are mixed, resulting in a two-band optical absorption spectrum: an intense B-band (or Soret band) in the near UV region and a weaker Q-band at lower energy.[68] The calculated energy position of the frontier orbitals of ZnP and the ZnTPP derivatives considered here are shown in Table 1. As these energies differ by only ±0.1 eV, it is expected that the optical absorption properties of ZnTPP-Ipa, ZnTMP-Ipa, *p*-ZnTCPP, and *m*-ZnTCPP will be nearly indistinguishable. This is in good agreement with previous UV−vis absorption measurements performed on the isolated molecules.[19]

Molecule-Oxide Energy Level Alignment. Parts a and b of Figure 3 show the molecular contribution to the UPS and IPS spectra from the functionalized $TiO_2(110)$ and $ZnO(11\bar{2}0)$ surfaces, respectively. The occupied states measured with UPS are plotted with energy less than zero, and the unoccupied states measured using IPS are plotted on the positive energy scale. To extract dye-related information, the contribution from the underlying oxides has been subtracted from the as-acquired spectra.[53] In these graphs, the zero of energy corresponds to the position of the Fermi level of the system.

The calculated DOSs are shown in Figure 3c. Here the unoccupied states were shifted 1.3 eV higher to compensate for DFT's well-known behavior of underestimating energy gaps. In addition, the zero of energy was shifted to align with the experimental Fermi level.

Keeping in mind that cross section effects are not taken into account in the DOSs of Figure 3c, comparison of the ab initio results to the measured occupied and unoccupied states of the chemisorbed molecules of Figure 3a and b provides a simple interpretation of the experimental electronic structure.

We can directly associate the calculated HOMOs and LUMOs to the highest occupied states and the lowest unoccupied states measured experimentally in Figure 3a and b. The strong emission features found experimentally ∼2 eV above the LUMOs and ∼2 eV below the HOMOs are attributed to functionalized phenyl states. The energy of these features follows the trends expected from the electronic donating or withdrawing character of the functional groups as was found in Figure 3c.

The energy positions of the HOMOs and LUMOs are chosen as centroids of the experimental features. The band edges are defined by extrapolating the valence and conduction band edges to the background level. From the energy position of the HOMOs and LUMOs of each ZnTPP derivative, the position of the $ZnO(11\bar{2}0)$ and $TiO_2(110)$ substrate band edges, and the vacuum level of both pristine and sensitized surfaces, a complete energy diagram at the chromophore−oxide interface can be drawn as shown in Figure 4.

Several important aspects of Figure 4 warrant comment. First, the HOMO−LUMO gap found from UPS and IPS, approximately 4.2 ± 0.2 eV for all four chromophores, represents the transport gap of the molecule. This value is ∼2 eV larger than the typical optical absorption gap reported for the same molecules.[18,19,22] This difference in energy is attributed in part to the binding energy of the exciton formed as a result of optical excitation.[53]

A second important point is that the energies of the HOMO and LUMO centroids with respect to the Fermi level is the same for both surfaces. A HOMO−Fermi level offset of 1.9 eV is compatible with a recently proposed model for energy alignment of UHV deposited organics at the surface of metal oxides.[70] This model further indicates that energy alignment could be tuned by altering the position of the Fermi level for a given oxide.[70]

Phrased in another way, for a given crystal surface (either ZnO or TiO_2), the alignment of the molecular orbitals with respect to the band edges of the substrate is identical for all four molecules. This is in good agreement with UV−visible absorption spectra and electrochemical redox potentials previously reported for similar molecules on both ZnO and

dx.doi.org/10.1021/jp307454y | *J. Phys. Chem. C* 2012, 116, 23921−23930

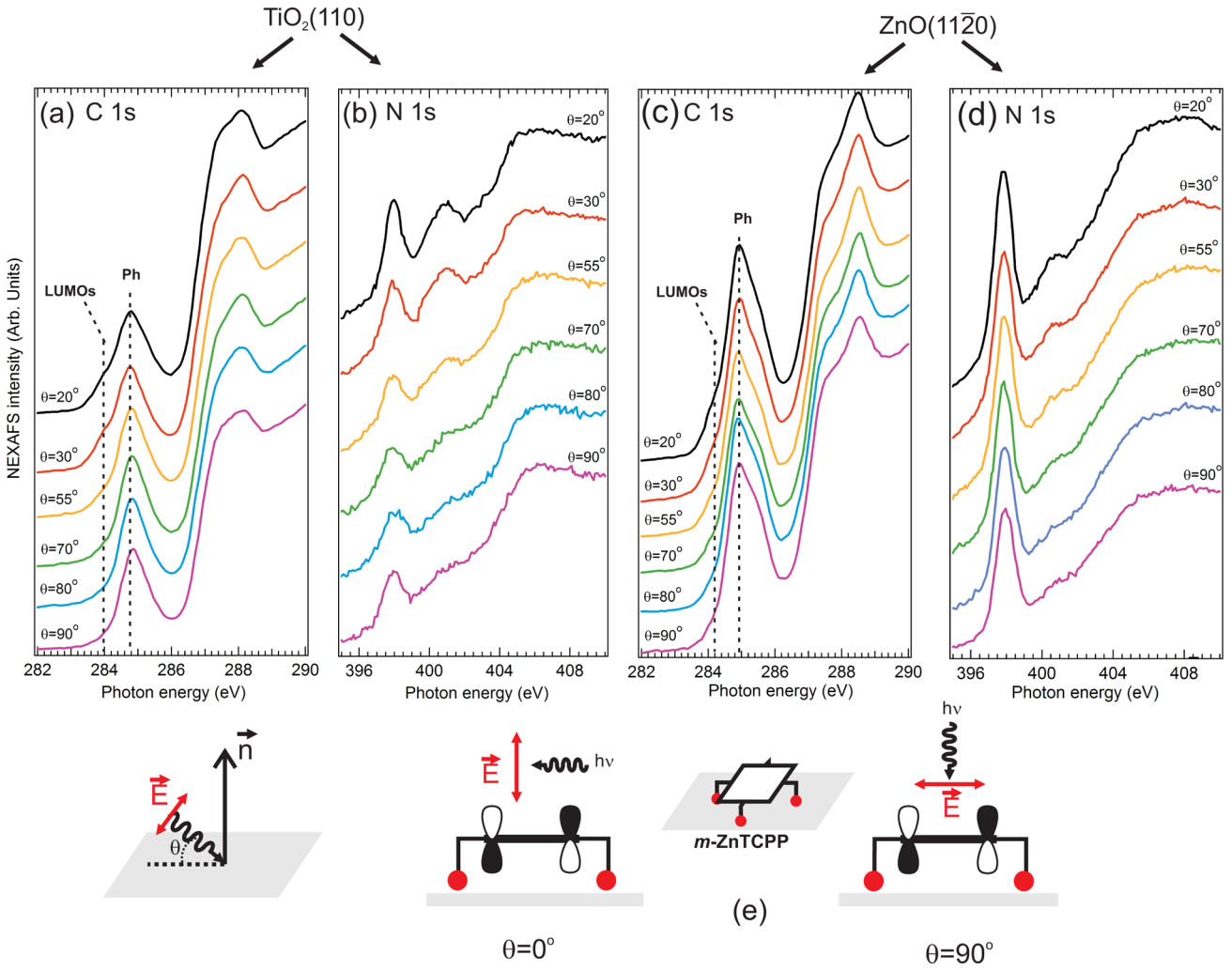

Figure 5. NEXAFS spectra of *m*-ZnTCPP adsorbed onto TiO_2(110) and ZnO(11$\bar{2}$0) at the C1s (a and c) and the N1s (b and d) edges as a function of the light incidence angle θ. The electric field is aligned with the [100] crystallographic direction for the TiO_2(110) surface and with the [100] direction for the ZnO(11$\bar{2}$0) surface.

TiO_2 nanoparticles,[18,19,22] and is consistent with the frontier orbitals being essentially independent of the meso-phenyl functionalization.

The results of this section indicate that the frontier orbitals involved in the photoexcitation process are nearly identical for the four ZnTPP derivatives. However, when adsorbed on wide band gap oxides, the optical absorption spectra and performances in device situations differ considerably.[19] This suggests that the geometry of the molecules with respect to the surface may play a key role in generating these differences.

Adsorption Geometry. *Molecular Orientation.* Figure 5 shows angle-dependent NEXAFS spectra of the C 1s and N 1s edges, measured from *m*-ZnTCPP-functionalized TiO_2(110) and ZnO(11$\bar{2}$0) surfaces. At the C 1s edge, the threshold feature at ~284 eV is attributed to transitions to the LUMOs located on the porphyrin macrocycle, while the feature at ~285 eV is attributed to the unoccupied phenyl states. For both surfaces, the intensity of the LUMO feature increases with decreasing angle between the photon polarization vector and the surface normal (as shown in Figure 5a and c). The intense phenyl feature at ~285 eV, however, does not display a strong dichroic behavior. At the N 1s edge (Figure 5b and d), a strong dichroism is observed and the intensities of all transitions are enhanced as the photon polarization vector nears alignment with the surface normal. The nature of the dichroism exhibited in both the C 1s and N 1s spectra indicates that *m*-ZnTCPP adsorbs with the porphyrin macrocycle parallel to the oxide surface for both crystals (as shown schematically in Figure 5e). The intensity of the NEXAFS transition of the ZnP ring LUMOs is maximized when the electric field vector of the incident light is parallel to the p orbitals composing the π^* system of the ZnP plane ($\theta = 0°$) and nearly suppressed when the electric field is perpendicular to the same p orbitals ($\theta = 90°$). The lack of dichroism of the ~285 eV feature of the C 1s spectrum is likely the result of a small tilt angle between the phenyls and the ZnP ring upon adsorption and/or near cancellation of the dichroism from orbitals on the phenyl rings.[71]

The NEXAFS spectra measured on the same surfaces sensitized with the *p*-ZnTCPP molecules indicate a very different adsorption geometry. The corresponding angle-dependent C 1s and N 1s edge NEXAFS spectra are shown in Figure 6. For both surfaces, no dichroism is observed at the C 1s edge (Figure 6a and d) or at the N 1s edge (Figure 6b and c). This can be interpreted either as a random orientation of the molecular species at the surface or as an adsorption geometry

dx.doi.org/10.1021/jp307454y | J. Phys. Chem. C 2012, 116, 23921−23930

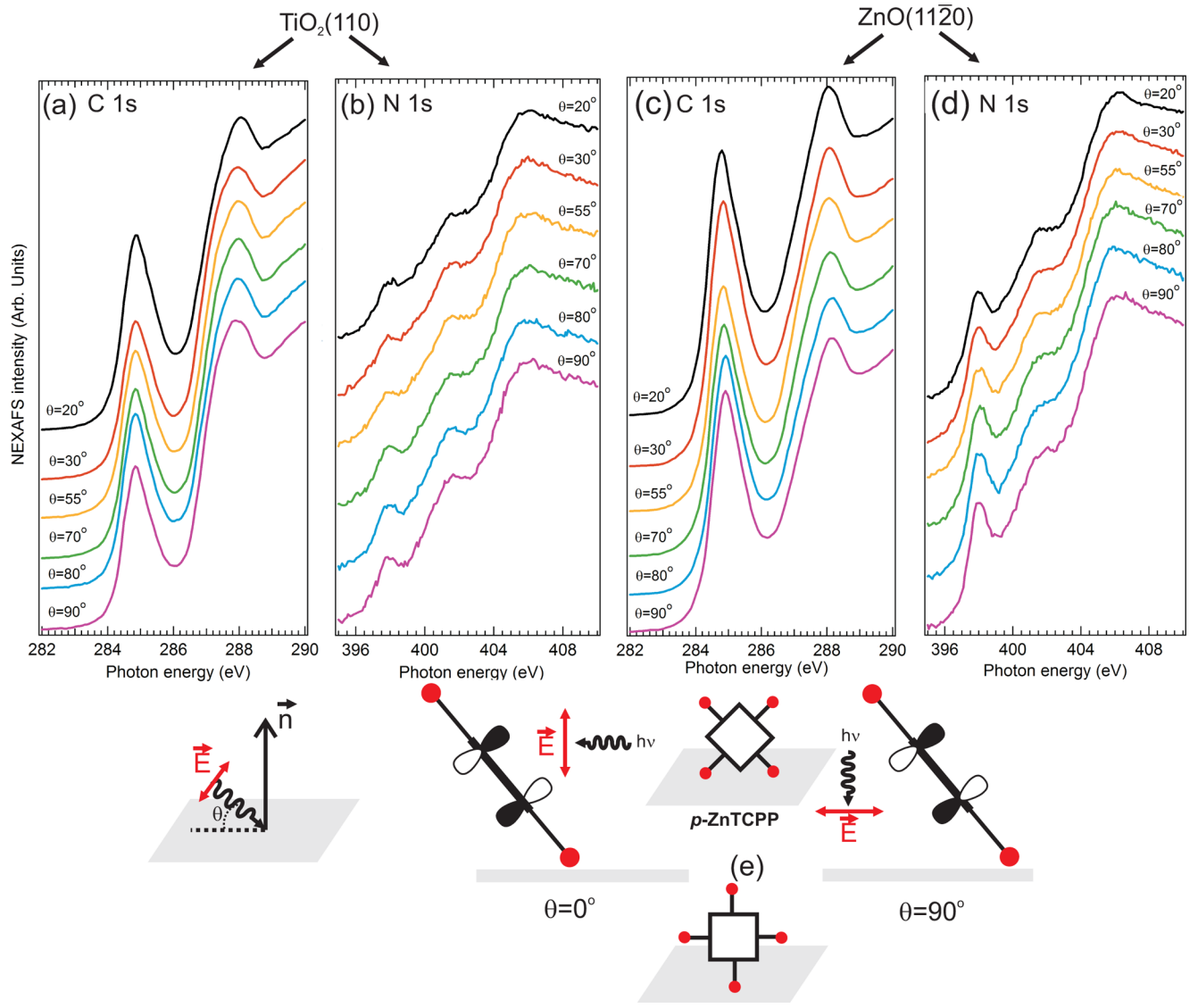

Figure 6. NEXAFS spectra of *p*-ZnTCPP adsorbed onto $TiO_2(110)$ and $ZnO(11\bar{2}0)$ at the C1s (a and c) and the N1s (b and d) edges as a function of the light incidence angle θ. The electric field is aligned with the [100] crystallographic direction for the $TiO_2(110)$ surface and with the [100] direction for the $ZnO(11\bar{2}0)$ surface.

where the ZnP plane makes an angle close to 50° with the surface normal. This latter case is illustrated in Figure 6e and could lead to an adsorption via one or two COOH anchoring groups.

Real-Space Images of m-ZnTCPP on $TiO_2(110)$. A more direct method to gain insights as to the geometry of molecular adsorbates on surfaces is to obtain real-space images of the system using scanning tunnel microscopy. STM images of the passivated and *m*-ZnTCPP functionalized $TiO_2(110)$ surfaces are reported in Figure 7. Figure 7a shows a close-up image of the ordered pivalate layer formed onto the $TiO_2(110)$ surface before sensitization. The adsorbed pivalic acid molecules are highlighted by a green circle. Figure 7c shows a large-area image of the passivated $TiO_2(110)$ after sensitization. The image is characterized by a regular array of small bright dots, with four-lobed clusters of brighter ovals interspersed. As indicated by the white squares, the former structures are identified as ordered pivalate species still present on the surface after sensitization. The newly present four-lobed features are interpreted as an image of the empty phenyl states of *m*-ZnTCPP adsorbed with their central ZnP ring parallel to the surface, as shown schematically in Figure 7d. Furthermore, it is apparent from Figure 7c, and the close-up image in Figure 7b, that *m*-ZnTCPP adsorbs at preferred binding sites, with a well-defined orientation with respect to the high symmetry directions of the surface, as well as with respect to each other. A model for the adsorption of *m*-ZnTCPP, and the pivalate species, is presented in Figure 7d. We propose that *m*-ZnTCPP binds to every other exposed surface 5-fold coordinated Ti row through the carboxylate species in the meta-position on the phenyl groups. The porphyrin rings are parallel to the surface, and the phenyl groups are essentially upright. The close-up image of Figure 7b suggests that adjacent *m*-ZnTCPP molecules are offset by one 5-fold Ti row, likely to reduce the repulsive interaction between phenyl groups of the neighboring molecules. This detailed picture of the *m*-ZnTCPP geometry on the $TiO_2(110)$ surface is entirely consistent with the NEXAFS results described in the previous section, and provides additional insight into the in-plane orientation of the molecules.

dx.doi.org/10.1021/jp307454y | *J. Phys. Chem. C* 2012, 116, 23921−23930

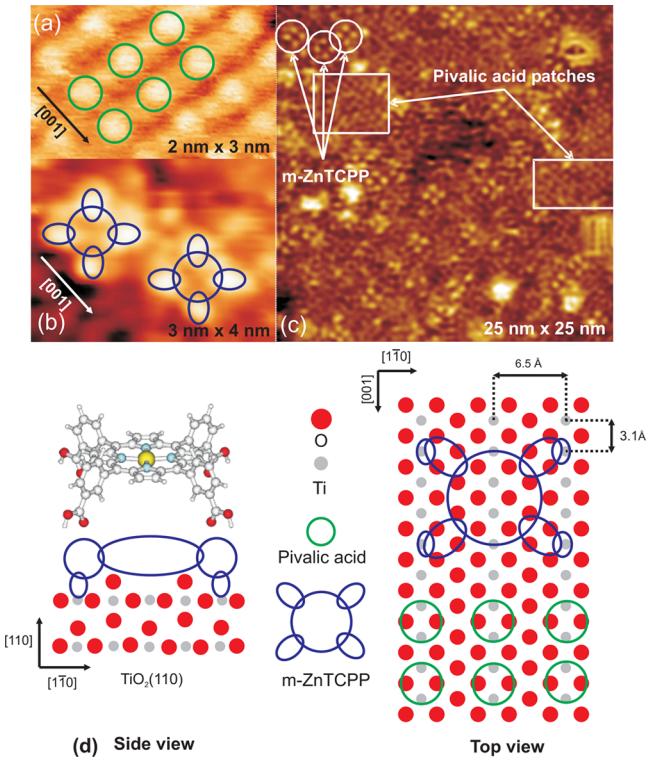

Figure 7. (a) Unoccupied states measured in STM (U = 1.6 V, I = 1 nA) of an ordered pivalate layer on a TiO_2(110) surface before sensitization. (b and c) STM images of a surface sensitized with *m*-ZnTCPP in unoccupied states (U = 2 V, I = 1 nA). (d) Adsorption geometries of both the pivalate layer and the *m*-ZnTCPP molecules are proposed in the side view and top view schematics of a TiO_2(110) surface.

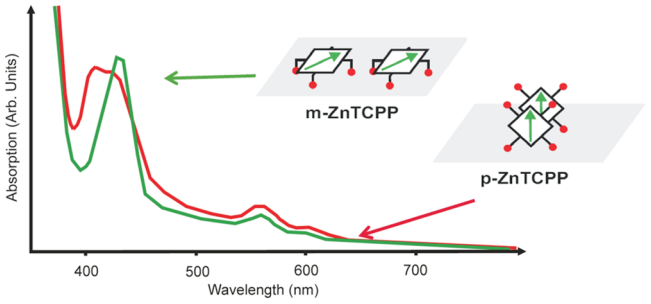

Figure 8. UV−visible absorption spectra measured on TiO_2 nanoparticles sensitized with *m*-ZnTCPP and *p*-ZnTCPP. Adapted from refs 18 and 19. The dipoles formed upon photoexcitation are indicated by green arrows.

Whereas imaging *m*-ZnTCPP on a TiO_2(110) surface gave reproducible results that allow detailed analysis of the molecular adsorption geometry, STM imaging of *p*-ZnTCPP bound to TiO_2(110) surfaces was not possible. Images of such surfaces show ordered structures from arrays of pivalate species accompanied by streaky features associated with the *p*-ZnTCPP species protruding more than a nanometer from the surface. This behavior is likely the result of *p*-ZnTCPP (rather than four) COOH anchoring groups with the plane of the porphyrin ring at a large angle from the plane of the surface whose orientation is perturbed during the imaging process. The contrasting behavior of *p*-ZnTCPP and *m*-ZnTCPP upon STM imaging confirms the large differences in binding geometry observed in the NEXAFS spectra of these two chromophores, suggesting that the interaction between adjacent dye molecules would be very different in the two cases.

Optical Properties and Exciton Delocalization. The different adsorption geometries for *m*-ZnTCPP and *p*-ZnTCPP when bound to TiO_2 can explain differences in the optical absorption properties found when TiO_2 nanoparticles are sensitized with these molecules. The UV−visible absorption spectra for these two molecules are shown in Figure 8 (adapted from previous work).[18,19] The absorption spectrum of *m*-ZnTCPP (Figure 8, green curve) is characterized by a strong Soret (or B) band centered at 424 nm and weaker Q-band features at 557 and 597 nm, respectively, and is essentially identical to what is found for both *m*-ZnTCPP and *p*-ZnTCPP in solution. In contrast, the Soret band of *p*-ZnTCPP (Figure 8, red curve) exhibits a strong blue-shifted component, generally attributed to H-aggregation: a face-to-face stacking of the excitation dipoles that are aligned in the plane of the ZnP macrocycle, as depicted in the lower inset of Figure 8. This sort of plane-to-plane coupling can occur only at the TiO_2 surface if the molecule is adsorbed with the porphyrin ring at a large angle with respect to the plane of the surface, as we find for *p*-ZnTCPP. This result rules out a totally random orientation of *p*-ZnTCPP at the surface, confirming that the NEXAFS data indicates upright bonding. This intermolecular dipole−dipole interaction is however absent for *m*-ZnTCPP because their porphyrin macrocycles, and hence the optical dipoles, are parallel to the surface (see upper inset in Figure 8).[72]

When combined with the results of our UHV studies, the absorption data provide direct evidence that the position (meta or para) of the COOH anchoring group on the phenyls of ZnTPP controls the adsorption geometry of the molecule on an oxide surface. The impact of adsorption geometry on device performance is illustrated by incident photon to current efficiency (IPCE) spectra for these molecules adsorbed on TiO_2 nanoparticles, as shown in Figure 9a. Details about these measurements can be found elsewhere.[18,19] It is clear that *m*-ZnTCPP-sensitized films exhibit a much larger efficiency over the full spectrum when compared to films sensitized with *p*-ZnTCPP. As our electronic structure measurements found essentially identical energy level offsets for these two systems, the large difference in IPCE cannot be explained from a simple energy alignment argument. Rather the difference likely has its origins in the molecule−surface bonding geometry. The tilted-upright geometry found for *p*-ZnTCPP increases the average macrocycle−surface distance as well as allows neighboring molecules to have parallel stacking of their porphyrin macrocycles. This opens a dipole-mediated intermolecular electronic channel that could compete with direct injection of a photoexcited electron into the TiO_2 substrate, and could contribute significantly to the observed loss of efficiency.

■ CONCLUSIONS

This work represents a comprehensive approach to understanding the ZnTPP derivative−oxide interfaces, that encompasses energy alignment, molecule−surface binding geometry, molecular packing, and their consequences on electronic de-excitation pathways of photoexcited electrons.

The electronic structure of the ZnTPP-Ipa, ZnTMP-Ipa, *p*-ZnTCPP, and *m*-ZnTCPP chromophores adsorbed both on TiO_2(110) and ZnO(11$\bar{2}$0) surfaces, measured using UPS and IPS, was interpreted using gas phase molecular DOS calculations. The energy alignment of the frontier orbitals

dx.doi.org/10.1021/jp307454y | J. Phys. Chem. C 2012, 116, 23921−23930

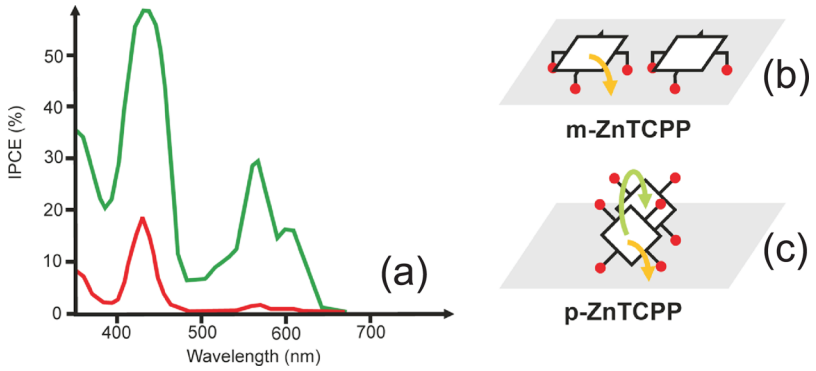

Figure 9. (a) Incident photon to current efficiency (IPCE) obtained from devices using TiO_2 nanoparticles sensitized with *m*-ZnTCPP and p-ZnCTPP (adapted from refs 18 and 19). (b) Main deexcitation channel for a photoexcited *m*-ZnTCPP: electron injection into the substrate conduction band. (c) Additional deexcitation channel enabled by the stacked geometry of the *p*-ZnTCPP molecules: exciton delocalization through dipole−dipole interaction.

relevant for photoexcitation with respect to the substrate band edges was directly extracted: (i) On a given substrate, the energy alignment of the frontier orbitals of the four ZnTPP derivatives is identical. (ii) The alignment of the ZnTPP derivatives with respect to the TiO_2 and ZnO band edges is shifted so as to keep the molecular levels at the same position with respect to the substrate Fermi level.

In addition, the effect on binding geometry of the functionalization of the phenyls with COOH anchoring groups either in meta- or para-position was studied. From NEXAFS spectroscopy, STM, and UV−visible spectroscopy, it is found that *m*-ZnTCPP adsorbs with its ZnP ring parallel to the oxide substrates, whereas *p*-ZnTCPP adsorbs in a geometry where the ZnP ring is at a large angle from the surface plane (with a possible tilt angle of ~50°). In the case of *m*-ZnTCPP, the main deexcitation channel for a photoexcited electron is through injection into the substrate conduction band. On the contrary, the upward adsorption geometry of *p*-ZnTCPP allows face-to-face stacking of the ZnP rings, opening a new deexcitation channel through dipole−dipole interaction.

AUTHOR INFORMATION

Corresponding Author

*E-mail: rangan@physics.rutgers.edu.

Notes

The authors declare no competing financial interest.

ACKNOWLEDGMENTS

The authors would like to thank Y. Lu for providing the ZnO(11$\bar{2}$0) epitaxial films and W. Wu for access to his STM. They would also like to thank Jonathan Rochford for the synthesis of compounds 1 and 2. Funding by the Division of Chemical Sciences, Geosciences, and Biosciences, Office of Basic Energy Sciences of the U.S. Department of Energy through Grant DE-FG02-01ER15256 is gratefully acknowledged. Certain commercial names are mentioned in this paper for purposes of example and do not constitute an endorsement by the National Institute of Standards and Technology.

REFERENCES

(1) Chou, J.-H.; Nalwa, H. S.; Kosal, M. E.; Rakow, N. A.; Suslick, K. S. In *The Porphyrin Handbook*; Kadish, K. M., Smith, K. M., Guilard, R., Eds.; Academic Press: San Diego, CA, 2000; Vol. *6*.
(2) Wasielewski, M. R. *Chem. Rev.* **1992**, *92*, 435−461.
(3) Harriman, A.; Sauvage, J.-P. *Chem. Soc. Rev.* **1996**, *25*, 41−48.
(4) Gust, D.; Moore, T. A.; Moore, A. L. *Acc. Chem. Res.* **1993**, *26*, 198−205.
(5) Tachibana, Y.; Haque, S. A.; Mercer, I. P.; Durrant, J. R.; Klug, D. R. *J. Phys. Chem. B* **2000**, *104*, 1198−1205.
(6) Montanari, I.; Nelson, J.; Durrant, J. R. *J. Phys. Chem. B* **2002**, *106*, 12203−12210.
(7) Tomizaki, K.-y.; Loewe, R. S.; Kirmaier, C.; Schwartz, J. K.; Retsek, J. L.; Bocian, D. F.; Holten, D.; Lindsey, J. S. *J. Org. Chem.* **2002**, *67*, 6519−6534.
(8) Campbell, W. M.; Burrell, A. K.; Officer, D. L.; Jolley, K. W. *Coord. Chem. Rev.* **2004**, *248*, 1363−1379.
(9) Nazeeruddin, M. K.; Humphry-Baker, R.; Officer, D. L.; Campbell, W. M.; Burrell, A. K.; Gratzel, M. *Langmuir* **2004**, *20*, 6514−6517.
(10) Loewe, R. S.; Ambroise, A.; Muthukumaran, K.; Padmaja, K.; Lysenko, A. B.; Mathur, G.; Li, Q.; Bocian, D. F.; Misra, V.; Lindsey, J. S. *J. Org. Chem.* **2004**, *69*, 1453−1460.
(11) Schmidt-Mende, L.; Campbell, W. M.; Wang, Q.; Jolley, K. W.; Officer, D. L.; Nazeeruddin, M. K.; Grätzel, M. *ChemPhysChem* **2005**, *6*, 1253−1258.
(12) Lo, C.-F.; Luo, L.; Diau, E. W.-G.; Chang, I.-J.; Lin, C.-Y. *Chem. Commun.* **2006**, 1430−1432.
(13) Hasselman, G. M.; Watson, D. F.; Stromberg, J. R.; Bocian, D. F.; Holten, D.; Lindsey, J. S.; Meyer, G. J. *J. Phys. Chem. B* **2006**, *110*, 25430−25440.
(14) Campbell, W. M.; et al. *J. Phys. Chem. C* **2007**, *111*, 11760−11762.
(15) Stromberg, J. R.; et al. *J. Phys. Chem. C* **2007**, *111*, 15464−15478.
(16) Muthiah, C.; Taniguchi, M.; Kim, H.-J.; Schmidt, I.; Kee, H. L.; Holten, D.; Bocian, D. F.; Lindsey, J. S. *Photochem. Photobiol.* **2007**, *83*, 1513−1528.
(17) Liu, X.; Liu, J.; Pan, J.; Andersson, S.; Sun, L. *Tetrahedron* **2007**, *63*, 9195−9205.
(18) Rochford, J.; Chu, D.; Hagfeldt, A.; Galoppini, E. *J. Am. Chem. Soc.* **2007**, *129*, 4655−4665.
(19) Rochford, J.; Galoppini, E. *Langmuir* **2008**, *24*, 5366−5374.
(20) Okujima, T.; Mifuji, A.; Nakamura, J.; Yamada, H.; Uno, H.; Ono, N. *Org. Lett.* **2009**, *11*, 4088−4091.
(21) Drain, C. M.; Varotto, A.; Radivojevic, I. *Chem. Rev.* **2009**, *109*, 1630−1658.
(22) de Tacconi, N. R.; Chanmanee, W.; Rajeshwar, K.; Rochford, J.; Galoppini, E. *J. Phys. Chem. C* **2009**, *113*, 2996−3006.
(23) Wasielewski, M. R. *Acc. Chem. Res.* **2009**, *42*, 1910−1921.
(24) Lin, C.-Y.; Lo, C.-F.; Luo, L.; Lu, H.-P.; Hung, C.-S.; Diau, E. W.-G. *J. Phys. Chem. C* **2009**, *113*, 755−764.
(25) Imahori, H.; Umeyama, T.; Ito, S. *Acc. Chem. Res.* **2009**, *42*, 1809−1818.

(26) Chang, C.-W.; Luo, L.; Chou, C.-K.; Lo, C.-F.; Lin, C.-Y.; Hung, C.-S.; Lee, Y.-P.; Diau, E. W.-G. *J. Phys. Chem. C* **2009**, *113*, 11524−11531.
(27) Walter, M. G.; Rudine, A. B.; Wamser, C. C. *J. Porphyrins Phthalocyanines* **2010**, *14*, 759−792.
(28) Maeda, C.; Kim, P.; Cho, S.; Park, J. K.; Lim, J. M.; Kim, D.; Vura-Weis, J.; Wasielewski, M. R.; Shinokubo, H.; Osuka, A. *Chem.—Eur. J.* **2010**, *16*, 5052−5061.
(29) Lee, C.-H.; Galoppini, E. *J. Org. Chem.* **2010**, *75*, 3692−3704.
(30) Kirmaier, C.; et al. *J. Phys. Chem. B* **2010**, *114*, 14249−14264.
(31) Martínez-Díaz, M. V.; de la Torre, G.; Torres, T. *Chem. Commun.* **2010**, *46*, 7090−7108.
(32) Yella, A.; Lee, H.-W.; Tsao, H. N.; Yi, C.; Chandiran, A. K.; Nazeeruddin, M.; Diau, E. W.-G.; Yeh, C.-Y.; Zakeeruddin, S. M.; Grätzel, M. *Science* **2011**, *334*, 629−634.
(33) Imahori, H.; Umeyama, T.; Kurotobi, K.; Takano, Y. *Chem. Commun.* **2012**, *48*, 4032−4045.
(34) Samuel, A. P. S.; Co, D. T.; Stern, C. L.; Wasielewski, M. R. *J. Am. Chem. Soc.* **2010**, *132*, 8813−8815.
(35) Lagref, J.-J.; Nazeeruddin, M.; Grätzel, M. *Inorg. Chim. Acta* **2008**, *316*, 735−745.
(36) van Amerongen, H.; Valkunas, L.; van Grondelle, R. *Photosynthetic Excitons*; World Scientific: Singapore, 2000.
(37) Aratani, N.; Osuka, A.; Cho, H. S.; Kim, D. *J. Photochem. Photobiol., C* **2002**, *3*, 25−52.
(38) Lu, H.-P.; Tsai, C.-Y.; Yen, W.-N.; Hsieh, C.-P.; Lee, C.-W.; Yeh, C.-Y.; Diau, E. W.-G. *J. Phys. Chem. C* **2009**, *113*, 20990−20997.
(39) Schnadt, J.; et al. *Surf. Sci.* **2003**, *540*, 39−54.
(40) Odelius, M.; Persson, P.; Lunell, S. *Surf. Sci.* **2003**, *529*, 47−58.
(41) Finnie, K. S.; Bartlett, J. R.; Woolfrey, J. L. *Langmuir* **1998**, *14*, 2744−2749.
(42) Vittadini, A.; Selloni, A.; Rotzinger, F. P.; Grätzel, M. *J. Phys. Chem. B* **2000**, *104*, 1300−1306.
(43) Nazeeruddin, M. K.; Humphrey-Baker, R.; Liska, P.; Grätzel, M. *J. Phys. Chem. B* **2003**, *107*, 8981−8987.
(44) Imahori, H.; et al. *J. Phys. Chem. A* **2011**, *115*, 3679−3690.
(45) Griffith, M. J.; James, M.; Triani, G.; Wagner, P.; Wallace, G. G.; Officer, D. L. *Langmuir* **2011**, *27*, 12944−12950.
(46) Chan, Y.-H.; Schuckman, A. E.; Peréz, L. M.; Vinodu, M.; Drain, C. M.; Batteas, J. D. *J. Phys. Chem. C* **2008**, *112*, 6110−6118.
(47) Persson, P.; Bergström, R.; Lunell, S. *J. Phys. Chem. B* **2000**, *104*, 10348−10351.
(48) Nilsing, M.; Persson, P.; Ojamäe, L. *Chem. Phys. Lett.* **2005**, *415*, 375−380.
(49) Nilsing, M.; Persson, P.; Lunell, S.; Ojamäe, L. *J. Phys. Chem. C* **2007**, *111*, 12116−12123.
(50) Angelis, F. D.; Fantacci, S.; Selloni, A. *Nanotechnology* **2008**, *19*, 424002.
(51) Pal, S. K.; Sundström, V.; Galoppini, E.; Persson, P. *Dalton Trans.* **2009**, 10021−10031.
(52) Formal chromophore names: Zn(II)-5-(3,5-dicarboxyphenyl) phenyl-10,15,20-triphenylporphyrin (ZnTPP-Ipa), Zn(II)-5-(3,5- dicarboxyphenyl)phenyl-10,15,20-trimesitylporphyrin (ZnTMP-Ipa), Zn(II)-5,10,15,20-tetra (4-carboxyphenyl) porphyrin (*p*-ZnTCPP), and Zn(II)-5,10,15,20-tetra(3-carboxyphenyl) porphyrin (*m*-ZnTCPP).
(53) Rangan, S.; Katalinic, S.; Thorpe, R.; Bartynski, R. A.; Rochford, J.; Galoppini, E. *J. Phys. Chem. C* **2010**, *114*, 1139−1147.
(54) Stöhr, J. *NEXAFS Spectroscopy*; Springer-Verlag: 1996.
(55) Cudia, C. C.; et al. *Surf. Sci.* **2006**, *600*, 4013−4017 (Berlin, Germany: Sept 4−9, 2005, Proceedings of the 23th European Conference on Surface Science).
(56) Schmidt, N.; Fink, R.; Hieringer, W. *J. Chem. Phys.* **2010**, *133*, 054703.
(57) The crystalline surfaces used in this study both have a 2-fold symmetry. In these measurements, the electric field of the polarized synchrotron light was aligned either with the [100] or [1$\bar{1}$0] crystallographic directions for TiO_2(110) and aligned either with the [1000] or [1$\bar{1}$00] crystallographic directions for ZnO(11$\bar{2}$0). As the 2-fold symmetry of the clean surfaces did not induce an azimuthal dichroism in the NEXAFS signal of the adsorbed species, results from only one of the crystallographic direction will be shown here.
(58) Sasahara, A.; Pang, C. L.; Onishi, H. *J. Phys. Chem. B* **2006**, *110*, 4751−4755.
(59) Ikeda, M.; Masatoshi, N.; Han, L.; Sasahara, A.; Onishi, H. *Langmuir* **2008**, *24*, 8056−8060.
(60) Schmidt, M. W.; et al. *J. Comput. Chem.* **1993**, *14*, 1347−1363.
(61) Becke, A. *Phys. Rev. A* **1988**, *38*, 3098−3100.
(62) Lee, C.; Yang, W.; Parr, R. *Phys. Rev. B* **1988**, *37*, 785−789.
(63) Becke, A. *J. Chem. Phys.* **1993**, *98*, 5648−5652.
(64) Schuchardt, K.; Didier, B.; Elsethagen, T.; Sun, L.; Gurumoorthi, V.; Chase, J.; Li, J.; Windus, T. *J. Chem. Inf. Model.* **2007**, *47*, 1045−1052.
(65) Walsh, P. J.; Gordon, K. C.; Officer, D. L.; Campbell, W. M. *J. Mol. Struct.: THEOCHEM* **2006**, *759*, 17−24.
(66) Liao, M.-S.; Scheiner, S. *J. Chem. Phys.* **2002**, *117*, 205−219.
(67) Liao, M.-S.; Bonifassi, P.; Leszczynski, J.; Huang, M.-J. *Mol. Phys.* **2008**, *106*, 147−160.
(68) Gouterman, M. *J. Chem. Phys.* **1959**, *30*, 1139−1161.
(69) Note that this number cannot be directly measured for this molecule but is an estimation from the comparison with the other ZnTPP derivatives.
(70) Greiner, M. T.; Helander, M. G.; Tang, W.-M.; Zhi-BinWang; Qiu, J.; Lu, Z.-H. *Nat. Mater.* **2012**, *11*, 76−81.
(71) Note that in the ideal case of *m*-ZnTPP adsorption with the ZnP macrocycle perfectly parallel to the surface, the N 1s NEXAFS peaks should be extinct for $\theta = 90°$. The absence of total extinction might have several causes. First, the surfaces have been sensitized in solution so as to obtain results close to the solar cell preparations and exposed to air briefly. It is possible that some of the nondichroic signal arises from atmospheric contaminants. Second, while at low coverage molecules can find adsorption sites suitable for a flat geometry, it is most likely that at high coverage some molecules will bind though only one or two COOH anchoring groups in a non-flat geometry. Finally, the surface roughness has to be considered: a rutile TiO_2(110) can be produced with large terraces; however, ZnO(11$\bar{2}$0) surfaces are characterized by smaller terraces, thus inducing more step edge adsorption sites. This might explain in part why the NEXAFS dichroism is much smaller on the ZnO(11$\bar{2}$0) surface. It can be however concluded from the NEXAFS results that, even at high coverage, the *m*-ZnTCPP are adsorbed in majority flat at the surface of both wide band gap semiconductors.
(72) The same behavior is observed when *p*-ZnTCPP and *m*-ZnTCPP are adsorbed on ZnO surfaces.